Hail climatologies for Sydney and Brisbane, Australia, derived from single-polarization radar and insurance claim data

Rob Warren, Hamish Ramsay, Steve Siems, Michael Manton

School of Earth, Atmosphere and Environment, Monash University, Melbourne, Victoria, Australia

Justin Peter, Roger Stone

International Centre for Applied Climate Sciences, University of Southern Queensland, Toowoomba, Queensland, Australia

Alain Protat

Bureau of Meteorology, Melbourne, Victoria, Australia

Contact: rob.warren@monash.edu

Introduction

- Severe hail storms are a significant hazard along the central east coast of Australia, with previous events causing billions of dollars' worth of damage
- Knowledge of the spatial distribution of these storms is thus relevant both to forecasters and the insurance industry
- Here, the hail hazard in the vicinity of the major cities of Sydney and Brisbane (Fig. 1) is quantified using observations from single-polarization radars which are verified against insurance claim data

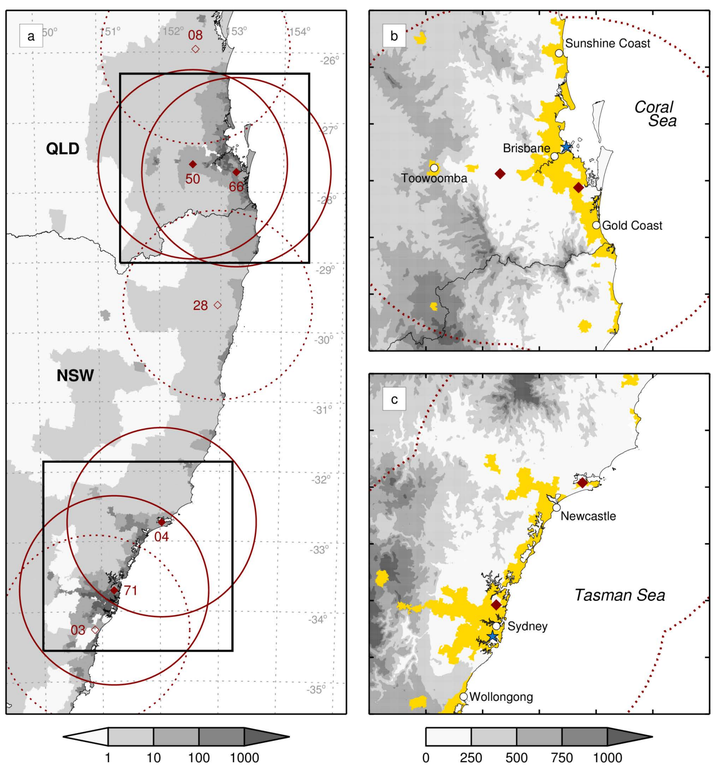

Figure 1. (a) Map of the central east coast of Australia showing the location of the two regions of interest (black squares). Shading shows the population density (people per km^2) while red diamonds and lines show, respectively, the locations and 150 km range rings of the radars used in this study. Filled diamonds and solid lines indicate primary radars; open diamonds and dotted lines indicate secondary radars. (b) Map of the Brisbane domain showing orography height (shading; m), areas of high population density (yellow shading; density ≥ 100 km^{-2}), major cities (white circles), primary radar locations (red diamonds) and coverage (red dotted lines), and sounding location (blue star). (c) As in (b) but for the Sydney domain. Both city domains are 300 x 300 km^2, with tick marks on the axes shown every 50 km.

Radar Data

- Archived data from seven single-polarization S-band radars (Table 1; Fig. 1) extracted for the period July 2009 to June 2015
- Reflectivities calibrated against Ku-band precipitation radars on board TRMM and GPM satellites (Warren et al. 2017)

Table 1. Details of the seven S-band radars used in this study. Symbols have the following meaning: λ = wavelength; ω = angular beam width; Δr = range gate spacing; N_θ = number of elevation sweeps in a volume scan; T = time between volume scans. All volume scans have an azimuthal beam spacing of 1°, and minimum and maximum elevation angles of 0.5 and 32°, respectively. Asterisks indicate primary radars. Note that the Newcastle radar was upgraded in 2013 and the Wollongong radar was replaced in 2011.

	ID	Name	Make	λ (cm)	ω (°)	Δr (m)	N_θ	T (min)
Brisbane	66	Brisbane*	Meteor 1500S	10.0	1.0	250	14	6
	50	Marburg*	WSR-74S	10.4	1.9	1000	15	10
	28	Grafton	WSR-74S	10.4	1.9	1000	15	10
	08	Gympie	DWSR-8502S	10.0	2.0	500	15	10
Sydney	71	Sydney*	Meteor 1500S	10.0	1.0	250	14	6
	04	Newcastle*	WSR-74S DWSR-74S	10.4 10.4	1.9 1.9	500 500	15 14	10 6
	03	Wollongong	WSR-74S DWSR-8502S	10.4 10.0	1.9 2.0	1000 500	15 14	10 6

- Reflectivity data from multiple radars combined to create a 3D mosaic with 1 km spatial and 5 min temporal resolution
- Following Langston et al. (2007), radar bins are weighted as

$$w = w_{\text{remap}} \times w_{\text{mosaic}} \times w_{\text{time}}$$

- Values first averaged to a common range gate spacing, $\Delta r_0 = 1$ km
- Remapping uses nearest neighbour interpolation in the range direction and bilinear interpolation in the azimuth–elevation plane
- For oversampled points close to the radar, the maximum reflectivity value is taken, as recommended by Langston et al. (2007)
- Spatially varying mosaic weights for each radar calculated based on size of radar sample volume relative to grid box size (Fig. 3):

$$w_{\text{mosaic}} = \left(\frac{r_{\max} - r}{r_{\max} - r^*} \right)^2$$

where $r_{\max} = 150$ km and $r^* = 2/\sqrt{\pi}\omega$ is the range at which the radar sample volume is equal to the grid box volume (1 km^3)

- Scans either side of analysis time used with linear time weighting
- Advection correction applied following Lakshmanan et al. (2006) with domain-wide velocity estimated using cross-correlation

Identifying Damaging Hail

- Reflectivity and sounding data used to compute daily accumulations of the maximum expected size of hail (MESH; Witt et al. 1998) for all days with radar data and at least 50 lightning strikes in the domain
- Building and contents hail-related claim and exposure data for insured properties within each domain provided by Suncorp Ltd.
- Total of 70 hail-claim days: 31 in Brisbane and 39 in Sydney
- For each claim day, grids of hail damage produced at 1 km spatial resolution for direct comparison with MESH (Fig. 2)

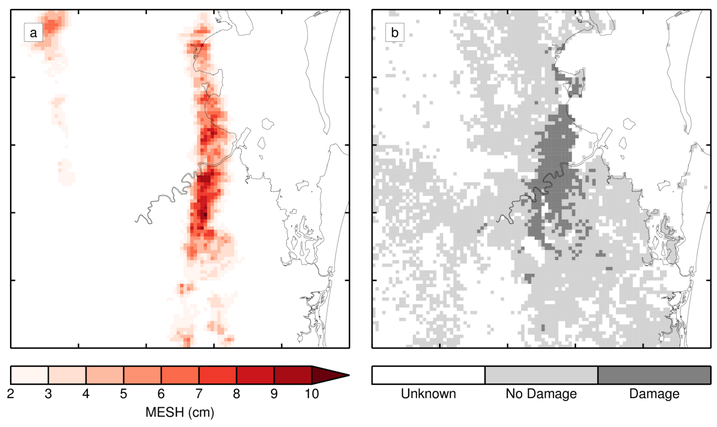

Figure 2. Fields of (a) accumulated MESH and (b) hail damage for 27 November 2014. The domain shown is 100 x 100 km^2 and approximately centred on Brisbane, with tick marks on the axes shown every 20 km. There is a pronounced spatial offset in this case, with the damage swath centred a few kilometres west of the highest MESH values. This is likely due to horizontal advection of hail during its descent.

- Contingency tables constructed by thresholding MESH at values from 0 to 8 cm in 0.5 cm increments using square spatial neighbourhoods with widths ranging from 1 to 25 km
- Equitable Threat Score (ETS) used to determine the optimal MESH threshold for identifying severe (i.e. damaging) hail
- MESH thresholds of 2.1 cm (Cinteno et al. 2012; Soderholm et al. 2016) and 3.5 cm (Fig. 3) used to identify, respectively, all hail events and severe hail events in the six-year dataset

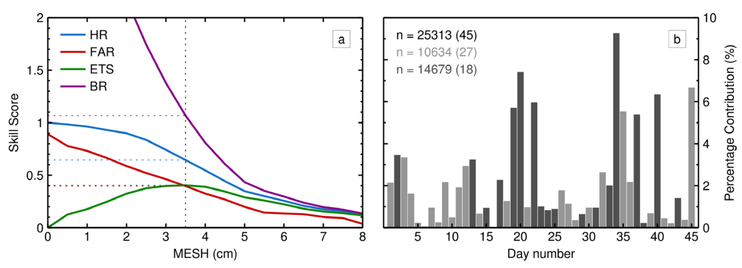

Figure 3. (a) Variation of skill scores (HR = Hit Rate, FAR = False Alarm Rate, ETS = Equitable Threat Score, and BR = Bias Ratio) with MESH for a neighbourhood width of 15 km. The optimal MESH threshold (3.5 cm) and corresponding skill scores are indicated by dotted lines. (b) Percentage contribution of each hail claim day to n, the total number of hit, miss, and false alarm grid boxes, at the optimal MESH threshold. Light and dark grey bars indicate events in the Sydney and Brisbane domains, respectively.

Frequency Maps

- Spatial distribution of hail in the Brisbane domain shows higher frequencies over the coastal plains, with a pronounced maximum south of the city (Fig. 4a,b), consistent with Soderholm et al. (2016)
- Hail frequencies are more spatially homogeneous in the Sydney domain, but show some relation to surface topography (Fig. 4c,d)

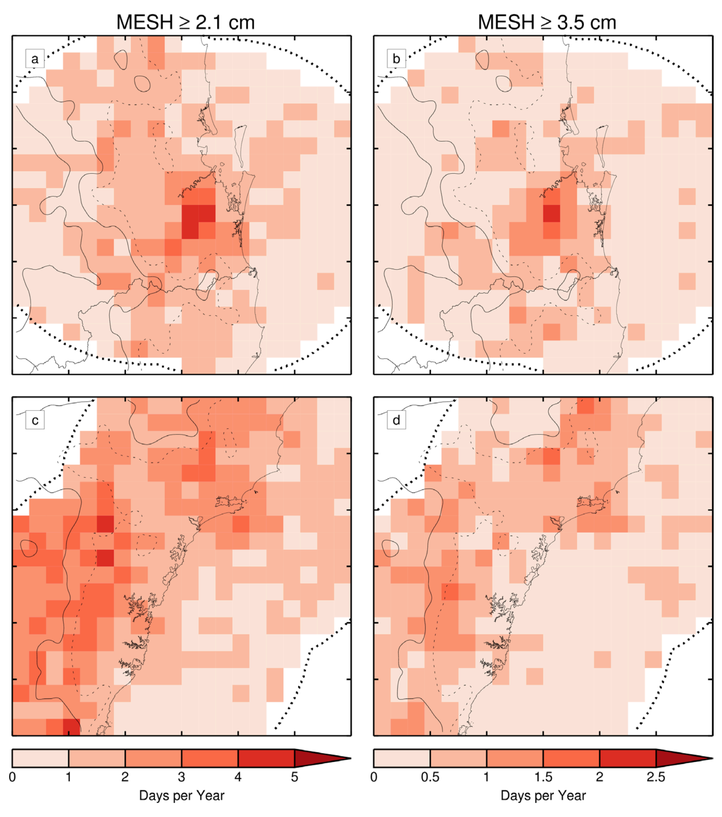

Figure 4. Maps showing the annual frequency of (left) all hail days (MESH ≥ 2.1 cm) and (right) severe hail days (MESH ≥ 3.5 cm) for the (top) Brisbane and (bottom) Sydney domains. Values are computed by counting the number of days for which the criterion is met within each 15 x 15 km^2 area, dividing by the total number of days in the six-year period (minus those with no radar data), and multiplying by 365. Thin dotted and solid lines show smoothed 250 and 500 m orography contours, respectively.

Seasonal and Diurnal Variations

- Seasonal and diurnal cycle of hail events (defined as five or more pixels above the MESH threshold) analysed for both domains (Fig. 4)
- In Brisbane, hail frequencies are maximised in spring and early summer, with 80 % of severe hail days occurring from September to January and 45 % in November–December alone
- Seasonal cycle in Sydney is less peaked and shifted later; just over 80 % of severe hail days occur between November and March
- In both locations hail frequency is maximised in the afternoon; over 80 % of severe events occurring between 1200 and 2000 LT

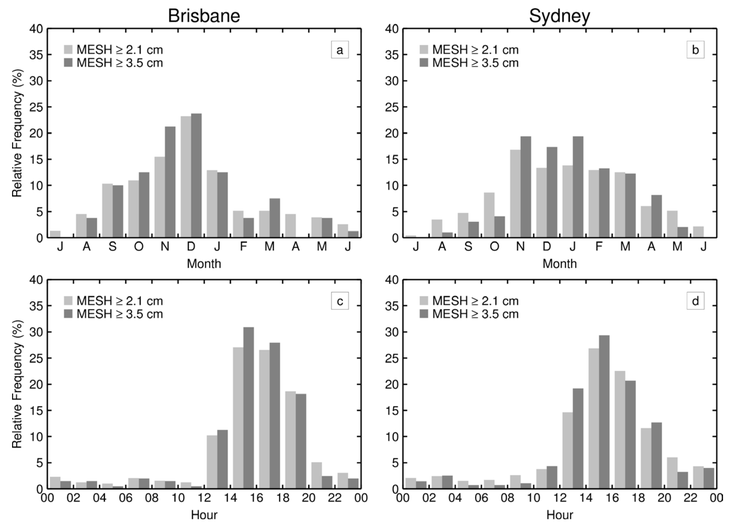

Figure 5. (top) Seasonal and (bottom) diurnal variations in all hail (light grey) and severe hail (dark grey) for the (left) Brisbane and (right) Sydney domains. Hours are in local time (LT).

Hail Storm Environments

- Soundings used to derive various convective parameters for thunderstorm (TS), non-severe hail (NH), and severe hail (SH) days in Brisbane and Sydney domains (Fig. 6)
- CAPE and maximum buoyancy increase with storm severity in both locations; largest difference is between NH and SH days in Sydney
- Increase in instability is primarily associated with steeper lapse rates in Brisbane and with higher parcel mixing ratios in Sydney
- Wind shear increases with storm severity in both locations; largest difference is between NH and SH days in Brisbane
- Composite parameter combining CAPE and shear provides the clearest indication of the potential for severe hail, but there is still considerable overlap between distributions

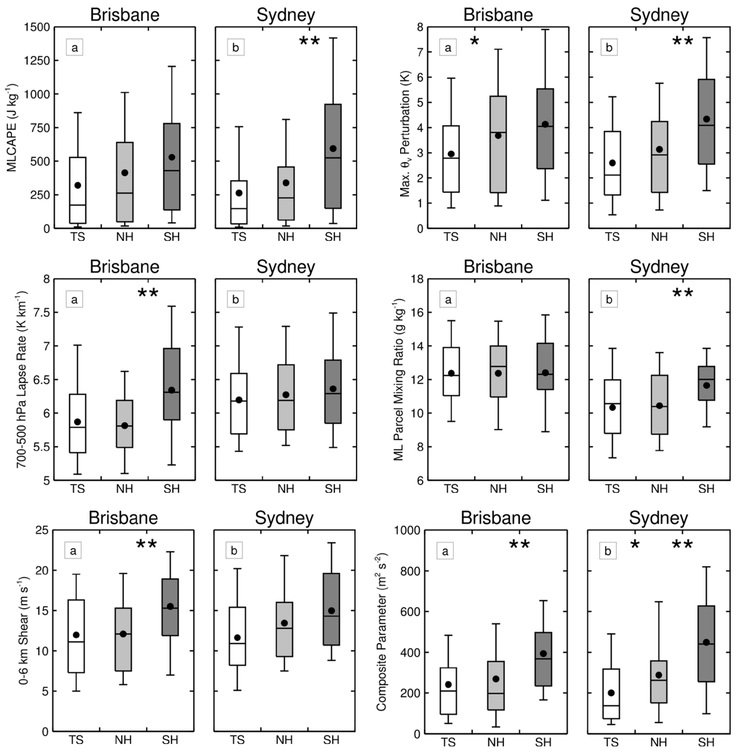

Figure 6. Box-and-whisker diagrams showing the distribution of various environmental parameters across thunderstorm (TS, white), non-severe hail (NH, light grey), and severe hail (SH, dark grey) days for the Brisbane and Sydney domains. Boxes show the interquartile range, whiskers show the 10th and 90th percentiles, horizontal lines show the median, and black dots show the mean. Single and double asterisks indicate where distributions are significantly different at the 5 % and 1 % levels, respectively (based on a permutation test with 1000 samples). Parameters shown are (a,b) mixed-layer (ML; 0–500 m) CAPE, (c,d) maximum virtual potential temperature (θ_v) perturbation, (e,f) 700–500 hPa lapse rate, (g,h) ML parcel mixing ratio, (i,j) 0–6 km shear, and (k,l) composite parameter computed as $\sqrt{2\text{CAPE}} \times$ shear.

References

Cintineo JL, Smith TM, Lakshmanan V, Brooks HE, Ortega KL. 2012. An objective high-resolution hail climatology of the Contiguous United States. *Wea. Forecasting*, **27**, 1235–1248.

Lakshmanan V, Smith T, Hondl K, Stumpf GJ, Witt A. 2006. A real-time, three-dimensional, rapidly updating, heterogeneous radar merger technique for reflectivity, velocity, and derived products. *Wea. Forecasting*, **21**, 802–823.

Langston C, Zhang J, Howard K. 2007. Four-dimensional dynamic radar mosaic. *J. Atmos. Oceanic Technol.*, **24**, 776–790.

Soderholm J, McGowan H, Richter H, Walsh K, Weckwerth T, Coleman M. 2016. The Coastal Convective Interactions Experiment (CCIE): Understanding the role of sea breezes for hailstorm hotspots in Eastern Australia. *Bull. Amer. Meteor. Soc.*, **97**, 1687–1698.

Warren RA, Protat A, Siems ST, Ramsay HA, Louf V, Manton MJ, Kane T. 2017. Calibrating ground-based radars against TRMM and GPM. *J. Atmos. Oceanic Technol.*, In Review.

Witt A, Eilts MD, Stumpf GJ, Johnson JT, Micthell ED, Thomas KW. 1998. An enhanced hail detection algorithm for the WSR-88D. *Wea. Forecasting*, **13**, 286–303.